

Shear-Wave Splitting and Implications for Mantle Flow Beneath the MELT Region of the East Pacific Rise

Cecily J. Wolfe* and Sean C. Solomon

Shear-wave splitting across the fast-spreading East Pacific Rise has been measured from records of SKS and SKKS phases on the ocean-bottom seismometers of the Mantle Electromagnetic and Tomography (MELT) Experiment. The direction of fast shear-wave polarization is aligned parallel to the spreading direction. Delay times between fast and slow shear waves are asymmetric across the rise, and off-axis values on the Pacific Plate are twice those on the Nazca Plate. Splitting on the Pacific Plate may reflect anisotropy associated with spreading-induced flow above a depth of about 100 km, as well as a deeper contribution from warm asthenospheric return flow from the Pacific Superswell region.

Observations of shear-wave splitting by the ocean-bottom seismometer (OBS) network of the MELT Experiment (1) describe the seismic anisotropy of the upper mantle beneath the southern East Pacific Rise. A shear wave passing through a homogeneous anisotropic layer splits into two waves with orthogonal polarizations and different wave speeds. Measurements of shear-wave splitting yield the direction of polarization ϕ of the fast shear wave and the delay time δt between the fast and slow shear waves (2, 3). Splitting parameters for the core phases SKS and SKKS reflect the path-integrated effects of upper mantle anisotropy beneath the receiving seismometer (4) and provide information on the orientation of the anisotropy as well as the combined effects of the thickness of the anisotropic region, the degree of anisotropy, and the isotropic velocity (5).

Because olivine, the most abundant mineral in the upper mantle, is anisotropic and develops lattice-preferred orientation in response to finite strain, splitting across the East Pacific Rise may be used to infer the pattern of flow-induced alignment of olivine grains (6–8) associated with mid-ocean ridge spreading. Both passive and dynamic models (9) of upwelling and divergence beneath spreading centers predict that flow in the upper 100 km of the mantle (8) should align the crystallographic a axes of olivine grains and produce measurable anisotropy (Fig. 1). Asthenospheric shear induced by absolute plate motion, large-scale mantle flow, or asthenospheric return flow may impart additional anisotropy to

deeper portions of the upper mantle. Splitting is also sensitive to the presence of mantle melt in vertically aligned cracks (Fig. 1), although a random distribution of melt in cracks or tubules would be isotropic and produce no splitting (7, 8).

We observe clear shear-wave splitting (Fig. 2) of SKS and SKKS phases from several earthquakes in the Kurile Islands and Indonesia (Table 1) recorded by the MELT network. Our splitting analysis follows stan-

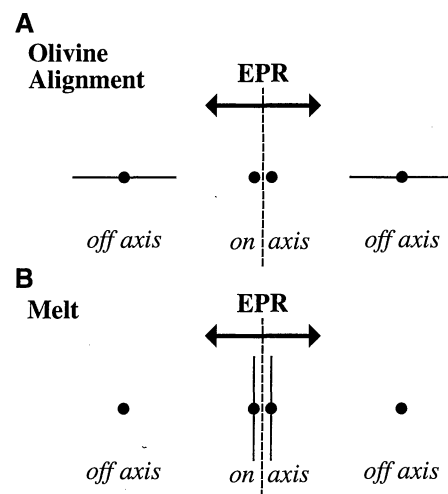


Fig. 1. Schematic of the expected shear-wave splitting patterns. (A) If anisotropy is dominated by the preferred alignment of olivine crystals, there should be no observable splitting on or near the rise axis, because mantle upwelling in this region induces a vertically oriented olivine a axis; farther off axis, mantle flow is predominantly horizontal and shear-wave splitting should be observed with fast direction ϕ parallel to spreading (arrows). (B) If anisotropy is dominated by melt in crack faces aligned parallel to the rise axis, splitting should be observed near the axis with ϕ parallel to the rise; because melting is confined to a region straddling the rise axis, the contribution from melt should decrease to zero far off axis.

dard methodology (3), as adapted (10) for deriving optimum splitting parameters from records of multiple events. Shear waves have good signal-to-noise ratio on the horizontal component records (1, 11) at frequencies of 0.04 to 0.1 Hz, which are equivalent to seismic wavelengths of 50 to 100 km. Splitting results were obtained for 18 instruments at 6 to 376 km from the rise axis on both the Pacific and Nazca Plates (Table 2 and Fig. 3). The splitting measurements combine data from one to six observations at each site.

For all observations, the fast polarization axis ϕ is consistently oriented nearly along the spreading direction of 103° measured clockwise from north (12). The mean value of ϕ at the MELT sites is 95° , and all but

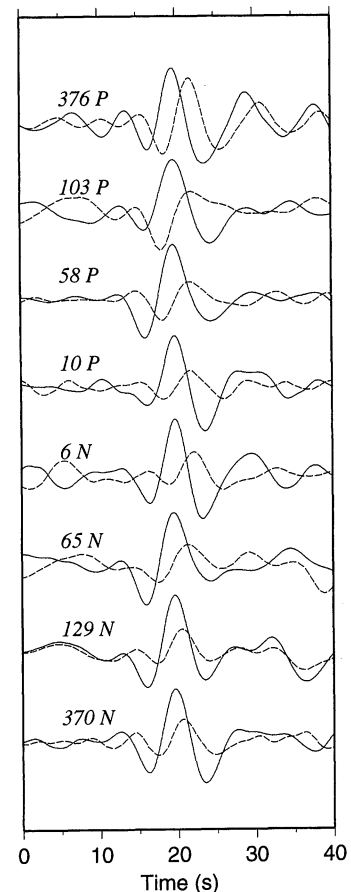


Fig. 2. Example SKKS waveforms from the earthquake of 25 December 1995, on radial (solid line) and transverse (dashed line) horizontal-component seismograms (bandpass filtered from 0.04 to 0.15 Hz); waveforms are aligned on the SKKS phase on the radial component. The consistent presence of energy on the transverse component is indicative of shear-wave splitting (2, 3); in the absence of anisotropy, the SKKS phase should be polarized in the radial direction with no energy on the transverse component. The distance from the rise axis, in kilometers, is shown; P denotes stations on the Pacific Plate, and N denotes stations on the Nazca Plate.

C. J. Wolfe, Department of Geology and Geophysics, Woods Hole Oceanographic Institution, Woods Hole, MA 02543, USA.

S. C. Solomon, Department of Terrestrial Magnetism, Carnegie Institution of Washington, Washington, DC 20015, USA.

*To whom correspondence should be addressed.

one estimate are within 15° of this value, an agreement consistent with the combined standard errors for ϕ and for instrument

orientation (13). The delay time δt between fast and slow shear waves is 0.8 to 1.4 s for instruments within 25 km of the rise axis.

Table 1. Earthquakes used for measuring shear-wave splitting parameters. BAZ is the back azimuth; that is, the direction of approach of the waves as seen at the MELT network, measured clockwise from north. M_S is the surface wave magnitude. Phases utilized included SKS for all earthquakes and SKKS phases for events 2 through 4.

Event no.	Date	Origin time (UT)	Latitude (°N)	Longitude (°E)	Depth (km)	BAZ	M_S
1	12/03/95	18:01:08	44.568	149.375	33	312°	8.0
2	12/25/95	04:43:25	-6.943	129.179	150	254°	6.7
3	01/01/95	08:05:12	0.724	119.981	33	259°	7.7
4	02/07/96	21:36:45	45.321	149.909	33	313°	7.0
5	02/17/96	05:59:30	-0.950	137.027	33	263°	8.1
6	03/22/96	03:24:20	51.221	178.695	20	323°	6.6

Table 2. Shear-wave splitting parameters at MELT OBS sites. N, Nazca Plate; P, Pacific Plate. The direction ϕ of shear-wave polarization is measured clockwise from north. Uncertainties for ϕ and δt are at one standard deviation.

Station	Latitude (°S)	Longitude (°W)	Rise distance (km)	ϕ (degrees)	δt (s)	Earthquakes used
S03	15.640	111.644	130N	94 ± 5	1.10 ± 0.10	1, 2, 4, 5
S04	15.740	112.507	45N	100 ± 2	0.97 ± 0.10	1-4
S05	15.822	112.867	10N	91 ± 8	0.80 ± 0.15	2, 4
S08	16.007	114.200	128P	98 ± 3	1.65 ± 0.13	1-5
S11	16.574	113.142	10P	104 ± 3	1.40 ± 0.20	1-4
S14	17.272	113.112	6N	96 ± 4	1.35 ± 0.18	1, 2, 4
S16	17.258	113.025	14N	85 ± 2	0.85 ± 0.10	1-4
S22	17.195	112.636	52N	91 ± 12	0.88 ± 0.22	2, 4
S23	17.171	112.502	65N	89 ± 6	1.00 ± 0.13	2, 4
S26	17.122	111.885	129N	75 ± 7	1.00 ± 0.18	2-4
S30	16.722	109.493	370N	108 ± 12	0.90 ± 0.13	2, 4, 6
S39	17.341	113.658	48P	89 ± 10	1.50 ± 0.35	1-3, 5
S40	17.349	113.754	58P	86 ± 3	1.65 ± 0.13	1, 2, 4, 5
S42	17.392	114.058	88P	91 ± 4	1.55 ± 0.15	1-3, 5
S43	17.411	114.209	103P	110 ± 8	1.70 ± 0.20	1-3
S45	17.491	114.957	179P	106 ± 8	2.20 ± 0.28	2
S48	17.786	116.926	376P	90 ± 5	1.85 ± 0.15	1-4
S50	17.467	113.316	10P	93 ± 4	1.25 ± 0.13	1-4

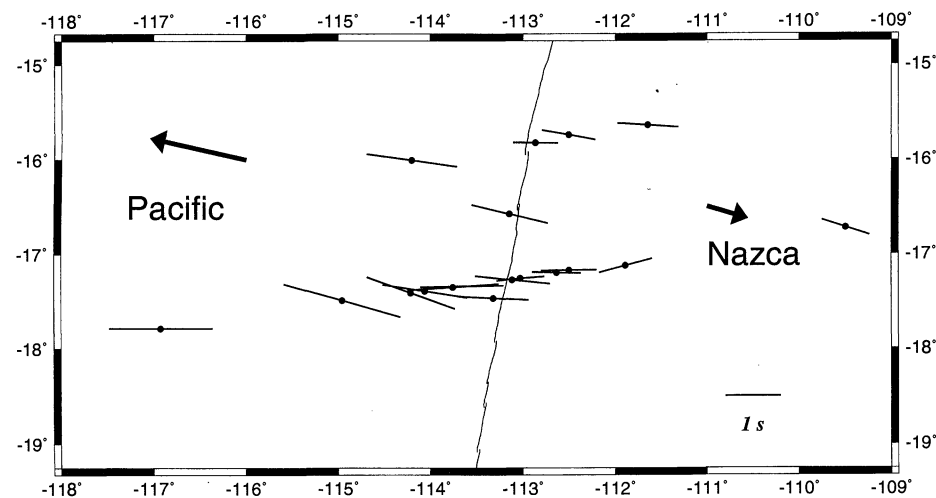


Fig. 3. Shear-wave splitting across the MELT array. Dots denote the position of the OBSs, and solid lines indicate the orientation of the fast direction ϕ , with the line length proportional to the delay time δt between fast and slow shear waves (Table 1). The rise axis is plotted as a solid line. Arrows indicate the magnitude and direction of absolute plate motion (20); the directions of absolute plate motion (20) and relative plate motion (12) are identical to within a few degrees in this region.

The delay time increases off axis on the Pacific Plate to values near 2 s but remains at about 1 s for instruments off axis on the Nazca Plate (Fig. 3 and Table 2).

The shear-wave splitting displayed in Fig. 3 is contrary to the predictions from simple flow and melting models (7, 8). Near axis, the fast direction ϕ of 95° and delays of about 1 s are inconsistent with anisotropy dominated by the presence of melt in crack faces aligned parallel to the ridge axis, which would produce a fast direction of approximately 5° (7). The near-axis splitting observations also differ from the negligible splitting predicted for a vertically oriented olivine a axis induced by mantle upwelling. The asymmetric splitting times off axis, with δt values as large as 2 s on the Pacific side, differ as well from model predictions (8) of smaller values (1 s) and symmetry about the rise axis. Furthermore, it is unlikely that the largest splitting delays on the Pacific Plate can be the result of anisotropy confined to the uppermost 100 km of the mantle. Typical values of percent anisotropy (5) from petrofabric measurements on mantle samples (14) are 3 to 5% (for a horizontal olivine a axis), yielding about 1 s of splitting for a 100-km-thick anisotropic layer. In addition, larger SKS anisotropy in the shallowest mantle would be inconsistent with Rayleigh-wave phase velocity measurements across the MELT network, which yield values for peak-to-peak anisotropy at a 25-s period of no more than 3 to 5% (15).

These arguments suggest that the largest splitting values reflect both a component of spreading-induced flow above a depth of 100 km and a deeper contribution, probably arising from upper mantle return flow (16) to the rise axis from the Pacific region. Both body-wave travel-time delays (11) and surface-wave phase velocities (15) across the MELT network display lower velocity values for the mantle on the Pacific side of the East Pacific Rise than on the Nazca Plate side. Asthenospheric return flow of anomalously warm mantle fed from the Pacific Superswell region (17) would explain the lower Rayleigh-wave velocities and more delayed body arrivals, as well as lesser rates of sea-floor subsidence with age (18) and a greater density of seamounts on the Pacific side of the rise axis (19). This scenario can also account for the splitting patterns seen in Fig. 3. On the Pacific side of the rise axis, greater asthenospheric shear imparted by the faster absolute motion of the Pacific Plate (20) and lower viscosities associated with higher temperatures, together with a component of return flow, can produce shear-wave splitting times that are 1 s greater than for the Nazca Plate side of the rise. We propose that splitting at the MELT

region reflects two anisotropic layers, both with ϕ oriented parallel to spreading. The upper layer, above a depth of about 100 km, is dominated by spreading-induced flow, which produces no splitting near the axis, where flow is predominantly vertical, but contributes to off-axis splitting as the flow diverges to a predominantly horizontal direction. The lower layer on the Pacific side consists of material experiencing return flow toward the ridge, but comparable return flow is more modest or absent on the Nazca side. Such an asthenospheric return flow could account for the 1-s splitting times seen on the rise axis, because the SKS phases in this study from sources to the west and northwest (Table 1) may sample the anisotropy induced by this flow at depths greater than 100 km.

REFERENCES AND NOTES

1. MELT Seismic Team, *Science* **280**, 1215 (1998).
2. L. P. Vinnik, R. Kind, G. L. Kosarev, L. I. Makeyeva, *Geophys. J. Int.* **99**, 549 (1989).
3. P. G. Silver and W. W. Chan, *J. Geophys. Res.* **96**, 16429 (1991).
4. SKS is a phase that propagates downward from the source as an S wave, converts to a P wave at the core-mantle boundary, travels through the fluid outer core, and then converts back to an S wave at the core-mantle boundary nearer to the point beneath the receiver. (An SKKS phase differs from SKS only in that the core path involves one underside reflection at the core-mantle boundary.) The conversion to P in the outer core removes any splitting accrued along the source side of the path, so when SKS or SKKS exits the outer core the converted shear wave is polarized in the direction radial to the source. Several lines of evidence [for example, C. Meade, P. G. Silver, S. Kaneshima, *Geophys. Res. Lett.* **22**, 1293 (1995)] suggest that neither Earth's lower mantle nor the transition zone between the upper and lower mantle contributes substantially to SKS or SKKS splitting. The dominant contribution to such splitting is the preferential alignment of the orthorhombic mineral olivine in the upper mantle beneath the receiving seismometer.
5. For a single anisotropic layer, the delay time will be $\delta t = L \delta\beta/\beta_0$, where L is the path length through the anisotropic material and is approximately equal to the layer thickness for near-vertically traveling SKS phases, and β_0 is the isotropically averaged shear velocity. $\delta\beta$ is the dimensionless anisotropy (the difference between the fast and slow shear velocities divided by β_0) and varies as a function of propagation direction ($100 \delta\beta$ is the percent anisotropy). Although the interpretation of shear-wave splitting measurements is generally made under the assumption of a single layer of anisotropic material, the more complicated case of multiple layers yields apparent splitting parameters that are functions of the anisotropy characteristics of individual layers [P. G. Silver and M. K. Savage, *Geophys. J. Int.* **119**, 949 (1994)]. Because the SKS and SKKS phases of our study sample only two back azimuths (Table 1), we cannot discount the possibility that there are multiple layers of distinct anisotropy, but the simple spreading-parallel splitting in Fig. 3 argues against such complexity.
6. N. I. Christensen, *Geophys. J. R. Astron. Soc.* **76**, 89 (1984).
7. J.-M. Kendall, *Geophys. Res. Lett.* **21**, 301 (1994).
8. D. K. Blackman *et al.*, *Geophys. J. Int.* **127**, 415 (1996); D. K. Blackman and J.-M. Kendall, *Philos. Trans. R. Soc. London Ser. A* **355**, 217 (1997).
9. In models of passive flow, viscous drag from the separating plates induces a broad zone, 100 km or more in width, of upwelling and melting centered beneath

the rise axis. In models of dynamic flow, the buoyancy from retained melt and the depleted mantle residuum, as well as a lower viscosity within the upwelling region, focus upwelling and melting within a narrower zone. See (8) for examples of these models.

10. C. J. Wolfe and P. G. Silver, *J. Geophys. Res.* **103**, 749 (1998).
11. D. R. Toomey *et al.*, *Science* **280**, 1224 (1998).
12. C. DeMets, R. G. Gordon, D. F. Argus, S. Stein, *Geophys. J. Int.* **101**, 425 (1990); *Geophys. Res. Lett.* **21**, 2191 (1994).
13. In the MELT Experiment, the horizontal seismometers were oriented on the basis of seafloor observations of seismic phases other than those utilized here (17); typical standard errors are 10° . Because we minimize the smaller eigenvalue of the covariance matrix of particle motion in solving for the SKS polarizations, small misorientations of the horizontals will map directly into a misorientation of ϕ but will not affect δt .
14. D. Mainprize and P. G. Silver, *Phys. Earth Planet. Inter.* **78**, 257 (1993).
15. D. W. Forsyth, S. C. Webb, L. M. Dorman, Y. Shen, *Science* **280**, 1235 (1998). Although models that would satisfy both the Rayleigh-wave results and shear-wave splitting are nonunique, the magnitude of Rayleigh-wave azimuthal anisotropy can be used

to infer an upper bound on the contribution to splitting from the shallow mantle, because the splitting directions ϕ are consistently parallel to spreading across the MELT network. If both Rayleigh-wave anisotropy and splitting were caused by anisotropy in a single shallow (<100 km in depth) layer in which olivine a axes were aligned parallel to the spreading direction, then Rayleigh waves would display high azimuthal anisotropy despite the effects of the larger Fresnel zone and path averaging.

16. J. Phipps Morgan and W. H. F. Smith, *Nature* **359**, 524 (1992).
17. M. K. McNutt and A. V. Judge, *Science* **248**, 969 (1990).
18. J. R. Cochran, *Geophys. J. R. Astron. Soc.* **87**, 421 (1986).
19. D. S. Scheirer, D. W. Forsyth, M.-H. Cormier, K. C. Macdonald, *Science* **280**, 1221 (1998).
20. A. E. Gripp and R. G. Gordon, *Geophys. Res. Lett.* **17**, 1109 (1990).
21. Supported by NSF under grants OCE-9402991 to the Department of Terrestrial Magnetism and OCE-9403697 to the Woods Hole Oceanographic Institution (WHOI). This is WHOI contribution 9711.

18 February 1998; accepted 21 April 1998

Mantle Discontinuity Structure Beneath the Southern East Pacific Rise from P-to-S Converted Phases

Yang Shen,* Anne F. Sheehan, Kenneth G. Dueker, Catherine de Groot-Hedlin, Hersh Gilbert

Receiver functions derived from teleseismic body waves recorded by ocean-bottom seismometers on the southern East Pacific Rise reveal shear waves converted from compressional waves at the mantle discontinuities near 410- and 660-kilometer depth. The thickness of the mantle transition zone between the two discontinuities is normal relative to the global average and indicates that upwelling beneath the southern East Pacific Rise is not associated with an excess temperature in the mantle transition zone.

The deep structure beneath mid-ocean ridges has been a subject of much debate and has direct implications for the mechanism of mantle upwelling beneath ridges as well as the pattern of global mantle circulation. Tomography studies by Su *et al.* (1) have suggested that slow seismic velocities, and hence anomalously warm mantle, exist to depths of 300 km and perhaps greater beneath mid-ocean ridges. This result implies that ridges are the product of deep-mantle upwelling associated with excess temperatures. Convection models that incorporate a platelike lithosphere predict that upwelling beneath ridges entrains

anomalously hot material from a thermal boundary layer either at the core-mantle boundary or at the base of the upper mantle (2). However, surface wave tomographic images constructed by Zhang and Tanimoto (3) indicate that mid-ocean ridges are shallow features, and hence the product of passive upwelling. The lack of a deep-ridge signature is consistent with models in which a low-viscosity asthenosphere acts to decouple upwelling beneath the ridge from flow in the deep mantle (4).

Lateral temperature variations in the upper mantle can be inferred from the depths of seismic discontinuities found on a worldwide basis near 410 and 660 km (5-9). The 410-km discontinuity has been identified with the transition from the α to β phase of $(\text{Mg,Fe})_2\text{SiO}_4$ and the 660-km discontinuity with the transition from γ - $(\text{Mg,Fe})_2\text{SiO}_4$ to perovskite plus magnesiowustite (10). The depths to the 410- and 660-km phase boundaries, respectively, increase and decrease with higher temperatures. Excess tempera-

Y. Shen, Department of Geology and Geophysics, Woods Hole Oceanographic Institution, Woods Hole, MA 02543, USA.

A. F. Sheehan, K. G. Dueker, H. Gilbert, Cooperative Institute for Research in Environmental Sciences (CIRES), University of Colorado, Boulder, CO 80309, USA.
C. de Groot-Hedlin, Scripps Institute of Oceanography, La Jolla, CA 92093, USA.

*To whom correspondence should be addressed: E-mail: yshen@whoi.edu